Biomed Microdevices (2016) 18: 116
DOI 10.1007/s10544-016-0139-y

An integrated microfluidic PCR system with immunomagnetic nanoparticles for the detection of bacterial pathogens

Irisappan Ganesh[1] · Buu Minh Tran[2] · Yonghee Kim[1] · Jaewon Kim[1] · Hua Cheng[3] · Nae Yoon Lee[2] · Sungsu Park[1]

Published online: 14 December 2016

Abstract There is growing interest in rapid microbial preconcentration methods to lower the detection limit of bacterial pathogens of low abundance in samples. Here, we report an integrated microfluidic PCR system that enables bacterial cells of interest in samples to be concentrated prior to PCR. It consists of two major compartments: a preconcentration chamber for the immunomagnetic separation of bacterial cells, and a PCR chamber for the DNA amplification of the concentrated cells. We demonstrate the feasibility of the system for the detection of microbial pathogens by preconcentrating the human pathogen *Escherichia coli* O157:H7, and also amplifying its DNA. The detection limit of *E. coli* O157:H7 in the PCR system is 1×10^3 CFU (colony forming unit)/mL. On-chip processing steps, including preconcentration and PCR steps, take less than two hours. Our system can serve as a rapid, specific, and quantitative platform for the detection of microbial pathogens in samples of large volume.

Irisappan Ganesh and Buu Minh Tran contributed equally to the work.

Electronic supplementary material The online version of this article (doi:10.1007/s10544-016-0139-y) contains supplementary material, which is available to authorized users.

✉ Nae Yoon Lee
nylee@gachon.ac.kr

✉ Sungsu Park
nanopark@skku.edu

[1] School of Mechanical Engineering, Sungkyunkwan University, Suwon 16419, Korea

[2] Department of BioNano Technology, College of BioNano Technology, Gachon University, Seongnam, Gyeonggi-do 13120, Korea

[3] Department of Chemistry and Nano Sciences (BK21 plus), Ewha Womans University, Seoul 03760, Korea

Keywords *Escherichia coli* O157:H7 · Microfluidic device · Immunomagnetic separation · On-chip PCR

1 Introduction

Polymerase chain reaction (PCR) is considered the most promising alternative to conventional methods of molecular diagnostics (Banada et al. 2009; Cho and Irudayaraj 2013; Pengsuk et al. 2013; Rodríguez-Lázaro et al. 2007; Setterington and Alocilja 2012; Varshney and Li 2007). Despite the high sensitivity of PCR, its application in samples requires extra labor-intensive and cumbersome steps for preconcentrating a small number of bacterial cells from a large volume of liquid sample, as well as providing DNA templates without any substance that inhibits polymerase reaction (Islam et al. 2006; Zhu et al. 2011).

To address the aforementioned issues, immunomagnetic separation (IMS) has often been used to concentrate bacterial cells present at low concentration (Chen et al. 2014; Zhu et al. 2011). However, it is suited to a small volume sample (e.g., 1 mL), which is far smaller than the large volume of enrichment culture (e.g., 250 mL) (Chen et al. 2014), and thus the pre-concentration effect is low. In recent years, there has been increasing interest in integrating IMS into microfluidic devices, to concentrate bacterial cells in a large volume of sample culture (Bu et al. 2008; Chen et al. 2014; Fedio et al. 2011; Pamme 2006; Roda et al. 2012; Xia et al. 2006). Microfluidic devices have become an excellent platform for detection, due to their speed and elevated level of integration and automation (Bao et al. 2008; Stachowiak et al. 2007). When integrated in a microfluidic device, IMS offers several advantages. It significantly increases the available surface area inside the microfluidic channel, which results in highly efficient interaction between bacterial cells and antibodies (Yang et al. 2006).

In this study, we describe the development of an integrated microfluidic PCR system with IMS for the enhanced detection of *Escherichia coli* O157:H7 in a large volume of samples. *E. coli* O157:H7 is one of the major pathogens causing diarrhea and acute kidney failure (Karch et al. 2005; Park et al. 1999). The microfluidic system **IMS chamber** consists of two major compartments: a preconcentration chamber (Magnetic Nanoparticle chamber), and a PCR chamber. The preconcentration chamber (MNP chamber) employs magnetic force to highly concentrate bacterial cells of interest in samples, while the PCR chamber amplifies DNA of the concentrated bacterial cells (Fig. S1).

2 Materials & methods

2.1 Design and fabrication of the microfluidic PCR system

To construct the system, all three layers (Fig.1a) were individually designed in AutoCAD software (Autodesk, San Rafael, CA, USA). The design of the top layer was printed on a transparency film and the film was used as a mask to transfer the design onto the layer of SU-8 negative-tone resist (Microchem, Westborough, MA, USA) in 200 μm thick on a Si wafer (4-in.). The developed structure of the wafer was used as a mold. The pattern from each mold was transferred into a polydimethyl siloxane (PDMS) (Sylgard 184) (Dow Corning, Midland, MI, USA) layer using soft lithography (Xia and Whitesides 1998). The top layer was comprised of arrays of pillars (diameter: 100 μm, height: 200 μm), with different spacing ranging from 150 to 750 μm (Fig.1a). The micropillar array with different spacing was installed to filter out food particles in various sizes. The design of the other two layers was individually printed using a DLP (digital light processing) 3D printer (DP 110) (Carima Co., Seoul, Korea) and each printout was directly used as a mold. Similarly, the pattern of each plastic mold was transferred onto the PDMS layer. The second layer contained an MNP chamber (W × L. × H: 2 × 3 × 1.5 cm). It was predicted using a computational model that bacterial capture efficiency decreased as the height of the MNP chamber increased. CFD simulation in the COMSOL Multiphysics® software (ver. 5.1) was used to analyze the behavior of Ab-MNPs at various heights (1–5 cm) while preserving the experimental conditions. The bottom layer contained a PCR chamber (W × L. × H : 4 × 6 × 1 mm). The height of the chamber was chosen by comparing temperatures at its various heights (1–10 mm) while thermocycling. The inlet and outlet holes (300 μm diameter) were punched with a biopsy punch. The layers were carefully aligned and bound to each other through O_2 plasma treatment at 90 watts for 30 s. After the O_2 plasma treatment, thermal curing in the oven for about 30 min at 80°C. Finally, prior to blocking, the system was sterilized in an autoclave at 121°C and the microchannel surface were passivated with bovine serum albumin (BSA) by flowing 100 μl of BSA in phosphate-buffered saline (pH 7.4) at 1.5 mg/mL into the PCR system, and incubating the chip at 80°C for 1 h, in order to inhibit non-specific absorption of PCR reagents into the PDMS surface (Besecker et al. 2010; Tran et al. 2013).

2.2 Microorganisms and cultivation

The bacterial strain used in this study was *E. coli* O157:H7 (ATCC 43894) (Bethesada, MD, USA). It was grown in Luria broth (LB) (Sigma) at 220 rpm and 37°C overnight. The culture was then 100-fold diluted with fresh LB, and incubated at 220 rpm and 37°C, until the optical density at 600 nm (OD_{600}) reached 1. Before preconcentration, the culture was diluted with PBS (pH 7.4).

2.3 Preparation of antibody conjugated magnetic nanoparticles (ab-MNPs)

MNPs (amine-modified iron oxide nanoparticles, 50 nm diameter) were obtained from Chemicell Co. (Berlin, Germany), while anti-*E. coli* O157:H7 antibody from goat was purchased from KPL, Inc. (Gaithersburg, MA, USA). For antibody conjugation, MNPs were first to react with 2.5% (*v*/v) glutaraldehyde solution (molar concentration) at RT for 1 h, and later washed completely with borate buffer (10 mM, pH 7.0) (Zhao et al. 2010). Then, the carboxyl group-terminated MNPs were mixed with anti-*E. coli* O157:H7 antibody (final conc. 50 μg/mL) in borate buffer, and incubated at 4°C overnight. Next, Ab-MNPs were first incubated in 0.1% bovine serum albumin (BSA) (Thermo Fisher Scientific, Waltham, MA, USA) in PBS to block unreacted aldehyde groups on Ab-MNPs at 4°C for 6 h, and later in sodium cyanoborohydride (final conc. 20 mg/mL) (Sigma-Aldrich) in borate buffer. Finally, antibody-conjugated MNPs were washed with Tris-HCl buffer (pH 7.5), and stored in PBS at 4°C until their use.

2.4 On-tube and on-chip bacterial preconcentration

The performance of IMS in tubes was compared with that of IMS in the microfluidic system. For on-tube IMS, 0.5 mL of PBS containing *E. coli* O157:H7 at different concentrations (10^2 to 10^4 CFU/mL) were mixed with 0.5 mL containing Ab-MNPs (1.3×10^{11} particles/mL) in Eppendorf® tubes (1.5 mL), and incubated at 1500 rpm (Thermoshaker) and 37°C for 20 min. The cells captured by Ab-MNPs were then concentrated by providing the magnetic field from a magnetic rack. Supernatants were used to count uncultured bacterial cells by the standard plate counting.

For on-chip preconcentration, 50 mL of PBS containing various concentrations (Final conc. 10^2–10^5 CFU/mL) of *E. coli* O157:H7 were mixed with anti-*E. coli* O157:H7

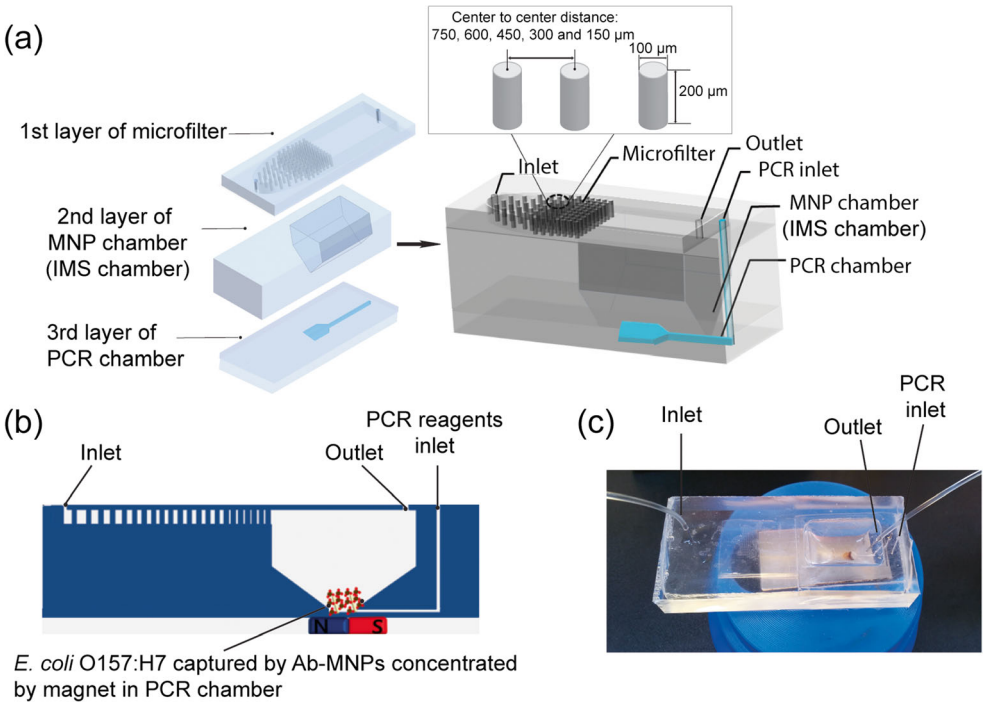

Fig. 1 Fabrication and operation of the integrated microfluidic PCR system with immunomagnetic nanoparticles (Ab-MNPs) for the detection of pathogens: a Assembly and design of the PCR system; b Principle of on-chip preconcentration: *E. coli* cells in samples bound with Ab-MNPs were captured by a magnet; **c** Operation of on-chip preconcentration

antibody-conjugated MNPs (final conc. 10^{12} particles/mL) in PYREX glass Erlenmeyer flasks (250 mL). The mixture was then incubated with gentle shaking at 200 rpm and 37°C for 20 min prior to loading the mixture into the PCR system, while the microchannel surface of the system was blocked with 1% BSA in PBS (pH 7.4) for 1 h prior to the addition of the mixture. To capture bacterial cells bound to Ab-MNPs, a magnetic field was applied to the MNP-concentrating chamber by locating the chip onto the top of a round neodymium magnet (diameter × height: 2.54 cm × 0.3 cm) with 1.5 T (Fig.1b). Figure 1c shows that the PCR system was connected to a syringe pump (Harvard Apparatus, Holliston, MA, USA), and a flow rate of 2 mL/min was maintained during sample injection (Mujika et al. 2009). Eluate collected from the chip was used to calculate bacterial capture efficiency. The bacterial cell number was determined by the standard plate counting method. The bacterial capture efficiency of each condition was calculated by the following formula: bacterial capture efficiency (%) = $(N_t - N_o)/N_t \times 100\%$, where N_t is the number of the total bacteria in a sample, and N_o is the number of un-captured bacteria in eluate.

2.5 Optimization of temperature of the PCR system

To perform PCR on the chip, the temperature of a PCR chamber was measured using an infrared (IR) camera (Thermovision A320) (FLIR Inc., Goleta, CA, USA) during the thermal cycling process. The 1 mm thick PCR system was placed on the heat block (10 × 10 cm) of a C1000 Touch thermal cycler (GeneTouch, Taoyuan City, Taiwan). Heat cycling was recorded and evaluated by ThermaCAM researcher 2.8 (FLIR Inc.). Nine spots on the chamber were randomly selected for temperature measurement. Time-dependent temperature variations were also evaluated to estimate the temperature of the PDMS substrate and PCR chambers during the thermal cycling process. Plot profiles of the nine spots were drawn based on data recorded continuously at millisecond duration in the first 20 min of the temperature parameter for the amplification reaction.

2.6 On-chip PCR on the integrated PCR system

Once the bacterial preconcentration step was completed in the integrated PCR system, two-temperature PCR was performed by adding 25 μL of PCR master mix into the PCR chamber via PCR reagents inlet. The PCR master mix containing 1× PCR buffer (20 mM Tris-HCl, pH 8.4, 50 mM KCl, 6 mM $MgCl_2$), dNTPs (0.2 mM), and *Taq* DNA polymerase (5 U/μL) was purchased from Promega (Madison, WI). The primers that were designed to amplify a 109-bp of *eaeA* gene coding intimin adherence protein in *E. coli* O157:H7 consist of a forward primer (CATTATTACGCCGGAAGATAAAATCC), and a reverse primer (GTCCGGGTATAACAACCATGAGTAAT). Two hundred microliters of mineral oil were then added to the chamber to cover PCR reagents, which prevents evaporation of the PCR mixture while thermal cycling. Two-temperature PCR (Dodson and Kant 1991; Ha and Lee 2015; Trinh et al. 2014) was performed by setting the temperature of the following parameters: 103°C for 10 min

as a bacterial cell lysis step, followed by 30 cycles of 103°C for 30 s, and 62°C for 30 s, and 76°C for 3 min for extension.

Amplified PCR products were confirmed by 1% TAE (50×) (Biosesang Inc., Korea) agarose gel electrophoresis using GelDoc EZ system (Bio-Rad). The fluorescence intensity of products on the gel was evaluated by ImageJ (NIH). 100-bp DNA ladder was from Takara Korea Biomedical Inc. (Korea), and agarose powder and loading buffer were purchased from BioShop Candada Inc. (Burlington, Canada) and DyneBio Inc. (Korea), respectively.

3 Results and discussion

3.1 Characterization of ab-conjugated magnetic nanoparticles (ab-MNPs)

The presence of antibody on Ab-MNPs was examined by observing fluorescence intensities of Alexa 488-tagged anti-goat antibody that was bound to anti-*E. coli* antibody from goat immobilized on MNPs (Fig. 2a). Bare MNPs without anti-*E. coli* antibody did not show any fluorescence is used as a control (Fig. 2ai), whereas Ab-MNPs conjugated with anti-*E. coli* O157:H7 antibody showed fluorescence (Fig. 2aii-2aiv). The strongest fluorescence was observed on Ab-MNPs (Fig. 2aiv) that had been previously conjugated with fifty micrograms of anti-*E. coli* O157:H7. Thus, fifty micrograms of antibody were chosen to be immobilized into MNPs (10^{12} particles) for further experiments.

The binding capability of Ab-MNPs to *E. coli* O157:H7 was confirmed by observing complexes of *E. coli* O157:H7 labelled using scanning electron microscopy (SEM). The image (Fig. 2b) showed bacterial cells in spherical forms (~ 1 μm diameter) surrounded by clusters of Ab-MNPs (50 nm in diameter), suggesting that Ab-MNPs can form complexes with bacterial cells through multivalent binding.

3.2 Effects of ab-MNP and bacteria concentrations and flow rate on bacterial capturing efficiencies

Figure 3 a shows that as the concentration of Ab-MNPs increases, the bacterial capturing efficiencies on the integrated PCR system increase. Although the highest capturing efficiency was obtained at 10^{13} particles per millilitre, Ab-MNPs at the concentration often accumulated in the tubing connected to the syringe due to its high density (data not shown), and the second best concentration (10^{12} particles/mL) was chosen for further experiments.

Figure 3b shows that flow rates negatively affected the bacterial capturing efficiency of the system. This is consistent with the result from computational fluidic dynamic (CFD) analysis (data not shown here). At 0.2 mL/min, the capturing efficiency of *E. coli* O157:H7 at 10^3 CFU/mL was the highest. However, the flow rate was too slow to handle a large volume of samples, such as 50 mL, within a short time. Thus, the flow rate of the preconcentrating step was chosen as 2 mL/min for further experiments.

Figure 3c shows that on chip bacterial concentration negatively affected the bacterial capturing efficiency of the system. This is probably because as the bacterial number in the sample increases, the number of Ab-MNPs bound with a single bacterium decrease. Thus, bacterial cells could be less affected by the magnetic field on the PCR system, and some of the cells might have been eluted out of the system. This problem could be overcome by diluting samples containing excessive numbers of bacteria of target, and then flowing the diluted samples into the PCR system. At 2 mL/min and 10^{12} Ab-MNPs/mL, we could detect as low as 10^2 CFU/mL by preconcentrating

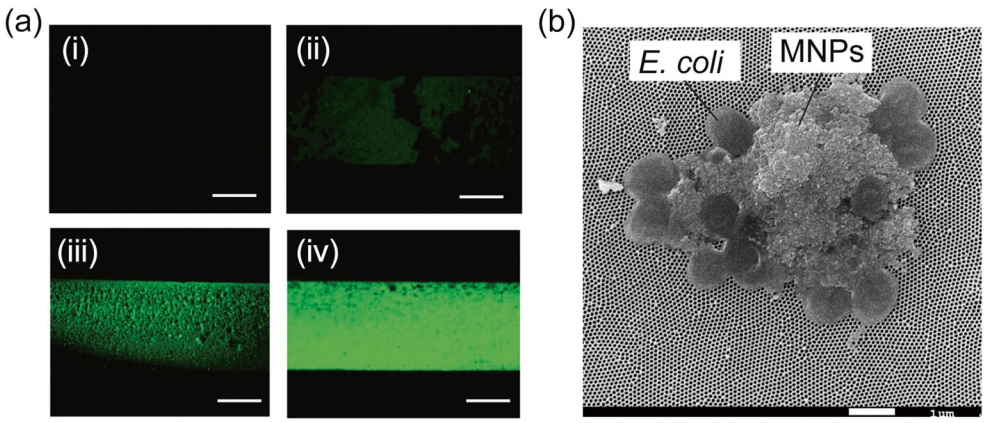

Fig. 2 Binding of Ab-MNPs to *E. coli* O157:H7: a Fluorescence images of anti-goat antibody conjugated with Alexa 488 (1.5 μg/mL) that were bound to MNPs (10^{12} particles/mL) previously conjugated with anti-*E. coli* O157:H7 antibody from goat at different concentrations: (i) no antibody; (ii) 1 μg/mL; (iii) 10 μg/mL; (iv) 50 μg/mL. Before imaging, twenty microliters of the mixture were loaded into the microchannel (1 mm width). Scale bar: 500 μm; b A scanning electron microscopic (SEM) image showing *E. coli* O157:H7 cells captured by Ab-MNPs. Scale bar: 1 μm

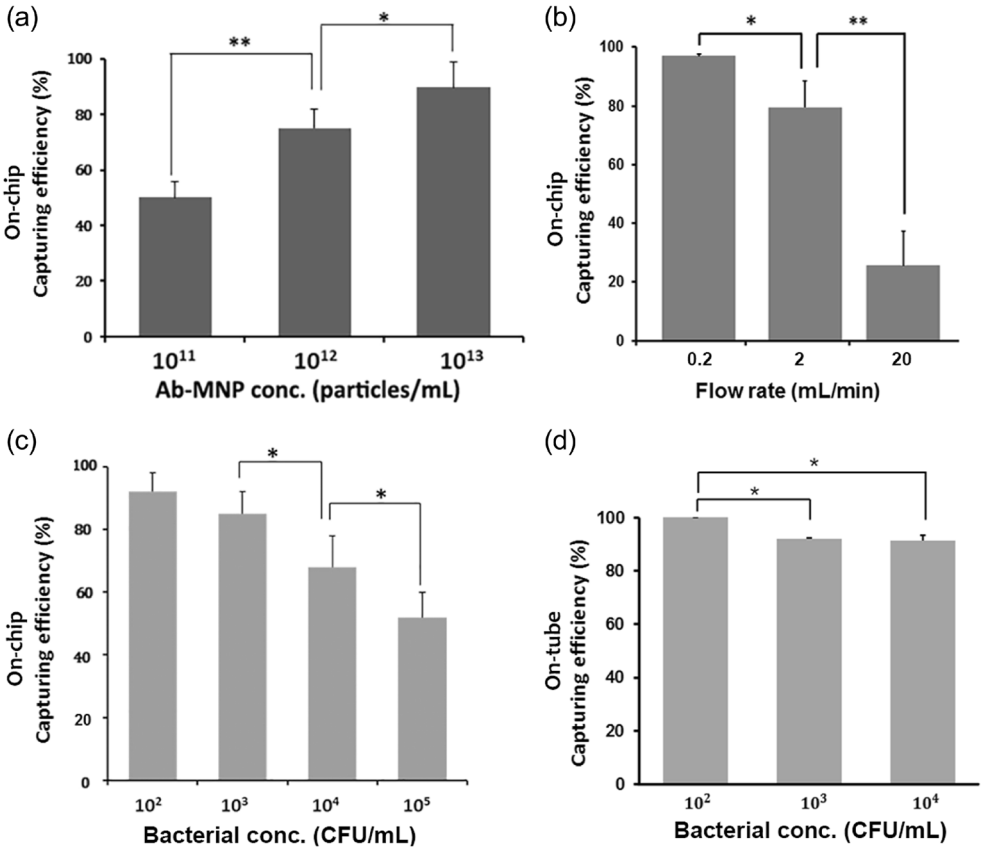

Fig. 3 Effects of Ab-MNP concentration, flow rate, and bacterial concentration on the on-chip bacterial capturing efficiency in 100 mL of PBS: a Capturing efficiency of *E. coli* O157:H7 (final conc. 10^3 CFU/mL) at a flow rate of 2 mL/min with Ab-MNPs at different concentrations (10^{11}–10^{13} particles/mL); b *E. coli* O157:H7 at 10^3 CFU/mL with Ab-MNPs (10^{12} particles/mL) at different flow rates (0.2–20 mL/min); c Ab-MNPs (10^{12} particles/mL) at 2 mL/min in the presence of *E. coli* O157:H7 at different concentrations (10^2–10^5 CFU/mL). d Ab-MNPs (10^{11} particles/ml) were used to detect *E. coli* O157:H7 (10^2–10^4 CFU/ml) by on-tube IMS; Student's t-test, $n = 3$. * $P < 0.05$, ** $P < 0.01$

bacterial cells of interest in 50 mL for 25 min, which is comparable to the results from our on-tube preconcentration experiments (Fig. 3d) and the previous reports (Fugier et al. 2015; Varshney et al. 2007). Although the on-tube preconcentration method needed the lower number (10^{11} particles/mL) of Ab-MNPs, it requires cumbersome liquid handling steps. Our results suggest that our on-chip bacterial preconcentration is more suitable for on-chip PCR and further automation than the on-tube bacterial preconcnetration method.

3.3 Temperature control for two-temperature PCR

The temperature on the surface of PDMS layer reached 95 ± 0.39°C from 29.2 ± 0.08°C in approximately 1 min, and it was maintained for 10 min before commencing the cycles. During the cycles, temperature of the PDMS surface at denaturation and annealing/extension steps were 94.1 ± 0.21°C (Fig. 4a) and 61.6 ± 0.13°C (Fig. 4b), respectively. The corresponding temperature accuracies, represented by the coefficient of variation (CV) values, were both 0.2% (n = 9). This indicates both highly uniform distribution of temperature over the measured surface, and low variability of heat transferred through PDMS. Figure 4c shows the PCR system placed on the thermal heat block, and the black rectangle indicates the PCR chamber under a heated condition. Figure 4d shows that the temperature profile of thermal cycles remained uniform throughout the entire thermal cycles.

Fig. 4d shows that the initial temperature before the thermal cycles remained at 103°C for 10 min to induce thermal lysis of bacterial cells, which enhanced the intensity of the target amplicons, as Fig. S2 shows. Thermal lysis for longer than 10 min did not increase the intensity, indicating that bacterial cells were fully ruptured within 10 min (Fig. S2). Similar thermal lysis steps were reported elsewhere (Ke et al. 2007; Liu et al. 2004). Taken together, the results suggest that temperature is well controlled on the PCR system.

3.4 On-chip two-temperature PCR for amplification of genomic DNA of *E. coli* O157:H7

To test if the microfluidic system can be combined with PCR, two-temperature PCRs were initially performed using the genomic DNA of *E. coli* O157:H7 as a template for the amplification prior to the use of bacterial cells on the system. Figure 5 shows that the targeted gene *eae* was successfully amplified from genomic DNA of *E. coli* O157:H7 at all concentrations (0.05–40 ng), suggesting that the integrated PCR system is comparable to the conventional PCR system.

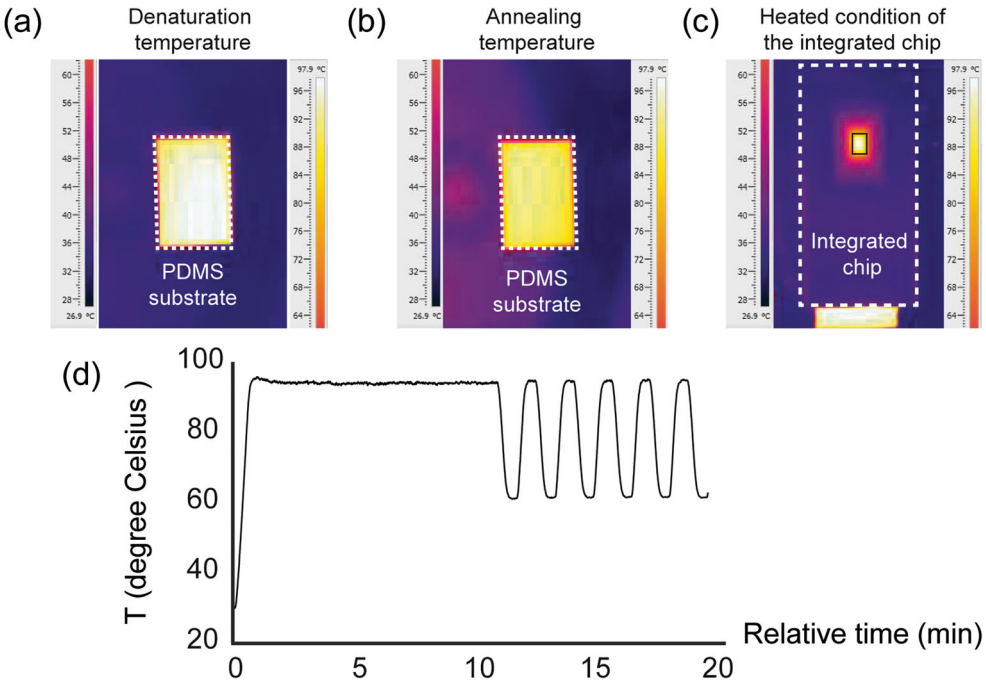

Fig. 4 Temperature measurement of the PDMS chamber. The temperature images were obtained using an IR camera during thermocycling: a Denaturation at 95°C; b Annealing/Extension at 62°C; c The entire integrated chip was placed on a heat block, and the black rectangle indicates the PCR chamber in a heated condition; d Temperature profile at the initial denaturation and the first 6 cycles

3.5 Integration of preconcentration and two-temperature PCR on the system

Figure 6 shows that as the cell concentration in the samples decreased, the intensity of the target amplicon decreased. The limit of detection of the integrated PCR system is 10^3 CFU/mL (lane 4 in Fig. 6). On-chip bacterial preconcentration, two-temperature PCR, and conventional gel electrophoresis took about 25 min, 1 h, and 30 min, respectively. Thus, all these steps were completed within 2 h. This is considerably quicker than other molecular amplification-based techniques (Naravaneni and Jamil 2005; Oblath et al. 2013; van Tongeren et al. 2011). The results suggest that the integrated PCR system is highly useful for the detection of bacterial cells at low abundance in a large volume of samples. Further improvement in

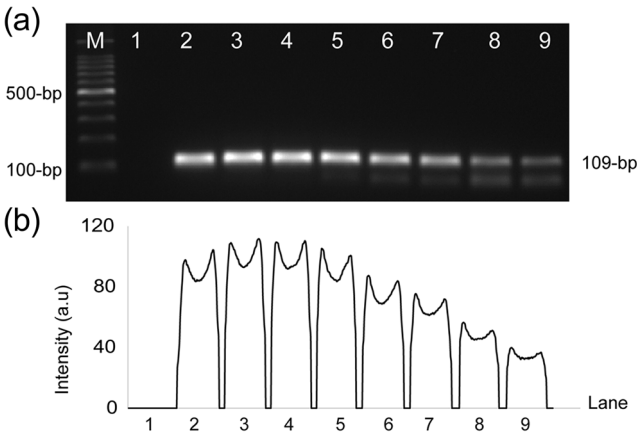

Fig. 5 Gel electrophoresis of the amplified products (109 bp) of *eae* gene in genomic DNA extracted from *E. coli* O157:H7. On-chip PCR was performed with genomic DNA (template) extracted from the microorganism: a Amplified products (109 bp) depend on the amounts of template DNA in PCR reaction. M Lane: 100 bp DNA ladder. Lane 1: negative control (no template DNA). Lane 2–8: PCR was performed with the template DNA at various concentrations: 40 ng (lane 2), 20 ng (lane 3), 10 ng (lane 4), 5 ng (lane 5), 1 ng (lane 6), 0.5 ng (lane 7), 0.1 ng (lane 8), and 0.05 ng (lane 9). Thermocycling and gel electrophoreis conditions are found in the Materials and Method section; b Respective fluorescence intensities of all the lanes (M-9)

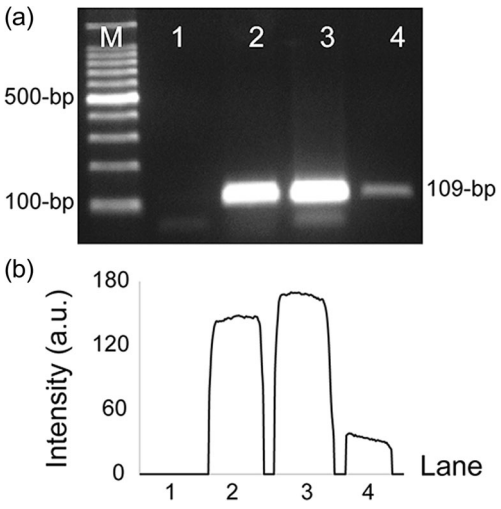

Fig. 6 Gel electrophoresis of the amplified products (109 bp) of *eae* gene in *E. coli* O157:H7 cells. On-chip PCR was performed with bacterial cells at various concentrations (10^3–10^5 CFU/mL) after on-chip preconcentration of samples (100 mL), using Ab-MNPs (10^{12} particles/mL) at a flow rate of 2 mL/min: a Amplified products (109 bp) from the microorganism in PBS. Lane M: 100 bp DNA ladder. Lanes 2–4: 10^5 CFU/mL, 10^4 CFU/mL, and 10^3 CFU/mL, respectively; b Respective fluorescence intensities of lanes (1–4)

preconcentration steps may lead us to detect bacterial cells at lower concentration than the current detection limit of the system.

4 Conclusion

Employment of chip-based detection techniques has discrete advantages that enhance the detection speed, miniaturization, and sensitivity. Here, the integration of preconcentration and DNA amplification of targeted pathogens in a large volume of samples was successfully demonstrated, by combining an IMS technique with two-temperature PCRs in a single microfluidic system. However, further improvements in the bacteria preconcentration step, as well as the DNA purification step, are still needed to lower the limit of detection in the integrated PCR system, to meet the detection requirements for the highly pathogenic microorganism, including *E. coli* O157:H7.

Acknowledgements This work was equally supported by the Public Welfare & Safety research program (2012M3A2A1051681), and the BioNano Health-Guard Research Center as Global Frontier Project (H-guard 2013M3A6B2078959) through the National Research Foundation (NRF) of Korea, funded by the Ministry of Science, ICT and Future Planning. The authors declare no commercial or financial conflict of interest.

References

P. P. Banada, K. Huff, E. Bae, B. Rajwa, A. Aroonnual, B. Bayraktar, A. Adil, J. P. Robinson, E. D. Hirleman, A. K. Bhunia, Biosens. Bioelectron. **24**, 1685–1692 (2009)

N. Bao, B. Jagadeesan, A. K. Bhunia, Y. Yao, C. Lu, J. Chromatogr. A **1181**, 153–158 (2008)

J. Besecker, K. A. Cornell, G. Hampikian, Sensors Actuators B Chem. **176**, 118–123 (2010)

M. Bu, T. B. Christensen, K. Smistrup, A. Wolff, M. F. Hansen, Sensors. Actuators A Phys. **145–146**, 430–436 (2008)

J. Chen, X. Shi, A. G. Gehring, G. C. Paoli, Int. J. Food Microbiol. **179**, 33–37 (2014)

I. H. Cho, J. Irudayaraj, Int. J. Food Microbiol. **164**, 70–75 (2013)

L. A. Dodson, J. A. Kant, Mol. Cell. Probes **5**, 21–25 (1991)

W. M. Fedio, K. C. Jinneman, K. J. Yoshitomi, R. Zapata, C. N. Wendakoon, P. Browning, S. D. Weagant, Int. J. Food Microbiol. **148**, 87–92 (2011)

E. Fugier, A. Dumont, A. Malleron, E. Poquet, J. Mas Pons, A. Baron, B. Vauzeilles, S. Dukan, PLoS One **10**, 1–15 (2015)

M. L. Ha, N. Y. Lee, Food Control **57**, 238–245 (2015)

M. A. Islam, A. E. Heuvelink, K. A. Talukder, M. H. Zwietering, E. de Boer, J. Food Prot. **69**, 2865–2869 (2006)

H. Karch, A. P.I.T, M. Bielaszewska, Int. J. Med. Microbiol **295**, 405–418 (2005)

C. Ke, A. Kelleher, H. Berney, M. Sheehan, A. Mathewson, Sensors Actuators B Chem. **120**, 538–544 (2007)

R. H. Liu, J. Yang, R. Lenigk, J. Bonanno, P. Grodzinski, Anal. Chem. **76**, 1824–1831 (2004)

M. Mujika, S. Arana, E. Castaño, M. Tijero, R. Vilares, J. M. Ruano-López, A. Cruz, L. Sainz, J. Berganza, Biosens. Bioelectron. **24**, 1253–1258 (2009)

R. Naravaneni, K. Jamil, J. Med. Microbiol. **54**, 51–54 (2005)

E. A. Oblath, W. H. Henley, J. P. Alarie, J. M. Ramsey, Lab Chip **13**, 1325–1332 (2013)

N. Pamme, Lab Chip **6**, 24–38 (2006)

S. Park, R. W. Worobo, R. A. Durst, Crit. Rev. Food Sci. Nutr. **39**, 481–502 (1999)

C. Pengsuk, P. Chaivisuthangkura, S. Longyant, P. Sithigorngul, Biosens. Bioelectron. **42**, 229–235 (2013)

A. Roda, M. Mirasoli, B. Roda, F. Bonvicini, C. Colliva, P. Reschiglian, Microchim. Acta **178**, 7–28 (2012)

D. Rodríguez-Lázaro, B. Lombard, H. Smith, A. Rzezutka, M. D'Agostino, R. Helmuth, A. Schroeter, B. Malorny, A. Miko, B. Guerra, J. Davison, A. Kobilinsky, M. Hernández, Y. Bertheau, N. Cook, Trends Food Sci. Technol. **18**, 306–319 (2007)

E. B. Setterington, E. C. Alocilja, Biosensors **2**, 15–31 (2012)

J. C. Stachowiak, E. E. Shugard, B. P. Mosier, R. F. Renzi, P. F. Caton, S. M. Ferko, J. L. van de Vreugde, D. D. Yee, B. L. Haroldsen, V. A. van der Noot, Anal. Chem. **79**, 5763–5770 (2007)

H. H. Tran, K. T. L. Trinh, N. Y. Lee, J. Chromatogr. B Anal. Technol. Biomed. Life Sci. **936**, 88–94 (2013)

K. T. L. Trinh, W. Wu, N. Y. Lee, Sensors Actuators B Chem. **190**, 177–184 (2014)

S. P. van Tongeren, J. E. Degener, H. J. Harmsen, Eur. J. Clin. Microbiol. Infect. Dis. **30**, 1053–1061 (2011)

M. Varshney, Y. Li, Biosens. Bioelectron. **22**, 2408–2414 (2007)

M. Varshney, Y. Li, B. Srinivasan, S. Tung, Sensors Actuators B Chem. **128**, 99–107 (2007)

N. Xia, G. M. Whitesides, Angew. Chem. Int. Ed. **37**, 550–575 (1998)

N. Xia, T. P. Hunt, B. T. Mayers, E. Alsberg, G. M. Whitesides, R. M. Westervelt, D. E. Ingber, Biomed. Microdevices **8**, 299–308 (2006)

L. Yang, P. P. Banada, M. R. Chatni, K. S. Lim, A. K. Bhunia, M. Ladisch, R. Bashir, Lab Chip **6**, 896–905 (2006)

L. Zhao, B. Yang, X. Dai, X. Wang, F. Gao, X. Zhang, J. Tang, J. Nanosci. Nanotechnol. **10**, 7117–7120 (2010)

P. Zhu, D. R. Shelton, S. Li, D. L. Adams, J. S. Karns, P. Amstutz, C. M. Tang, Biosens. Bioelectron. **30**, 337–341 (2011)